J. Fluid Mech. (1999), *vol.* 385, *pp.* 63–78. Printed in the United Kingdom

On Rayleigh's computation of the 'end correction', with application to the compression wave generated by a train entering a tunnel

By M. S. HOWE

Boston University, College of Engineering, 110 Cummington Street, Boston, MA 02215, USA

(Received 23 June 1998 and in revised form 30 October 1998)

Rayleigh's (1926, Appendix A) method for the approximate calculation of potential flow from the open end of a semi-infinite flanged cylinder is applied to obtain analytical representations of Green's function describing the generation of sound waves within a flanged cylinder by sources located in the neighbourhood of the open end. Detailed results are given for the circular cylinder considered by Rayleigh and extension made to a flanged cylinder of rectangular cross-section. The validity of various approximations is assessed by comparison with the exact solution available (by the method of conformal transformation) for potential flow from a two-dimensional, flanged duct. The results are used to compare the profiles and the pressure gradients of compression waves generated when a high-speed train enters tunnels of circular and rectangular cross-sections.

1. Introduction

The wavelengths λ_n of standing acoustic waves in a rigid, narrow tube of length ℓ, open to the atmosphere at one end, are given by

$$\lambda_n = \frac{4(\ell + \ell')}{2n-1}, \quad n = 1,\ 2,\ \ldots\ ,$$

where the additional length ℓ' is called the 'end correction'. For a circular cylindrical tube of radius R with an 'unflanged' open end, $\ell' \approx 0.61R$, and $\ell' \approx 0.82R$ for a flanged end, which is flush with an infinite, plane rigid wall (Rayleigh 1870, 1926). The magnitude of the end correction depends on the inertia of fluid set in motion outside the tube in the neighbourhood of the opening, and the resonance frequencies are the same as those predicted by elementary arguments when the pressure is assumed to vanish at a distance ℓ' beyond the end.

Rayleigh gave the following interpretation of the end correction. Consider a long tube of cross-sectional area $\mathscr{A}$ with a freely moving piston of equal area that advances at infinitesimal Mach number towards the open end, so that the fluid motion may be regarded as incompressible. For an ideal fluid, of uniform mean density ρ_o, the motion is also irrotational, with velocity potential $\phi^*(\boldsymbol{x})$, say. If the piston moves at unit speed, ϕ^* is a solution of Laplace's equation whose normal derivative (directed into the fluid) satisfies $\partial\phi^*/\partial n = 1$ on the face of the piston and vanishes on the walls of the tube. Then the energy T of the incompressible motion is entirely kinetic, and

$$T \equiv \tfrac{1}{2}\rho_o \int_V (\nabla\phi^*)^2 \,\mathrm{d}^3\boldsymbol{x} = \tfrac{1}{2}\rho_o \mathscr{A}(\ell + \ell'), \tag{1.1}$$

where the integration is over the fluid V, outside the tube and within the tube between the open end and the piston, and $\ell \gg \mathscr{A}^{1/2}$ is the instantaneous distance of the piston from the open end.

Any other possible velocity distribution of the incompressible motion produced by the piston, that satisfies the same boundary conditions on the walls and piston, is necessarily rotational, with velocity $\nabla\phi^* + \boldsymbol{v}$, where curl $\boldsymbol{v} \neq \boldsymbol{0}$. Kelvin's theorem (Lamb 1932, §45) asserts that the kinetic energy T' of this motion cannot be less than the kinetic energy (1.1) of the irrotational flow, a result that can be expressed in the form

$$\ell + \ell' \leqslant \frac{2T'}{\rho_o \mathscr{A}}. \tag{1.2}$$

Rayleigh (1870, 1926) exploited this minimum property to estimate the value of ℓ' by first calculating T' from a solution of the piston problem containing one or more disposable parameters, whose values were then chosen to make T' a minimum.

The potential function $\phi^*(\boldsymbol{x})$ is defined only to within an arbitrary, additive constant. Take the origin O of rectangular coordinates $\boldsymbol{x} = (x, y, z)$ in the plane of the open end, with the negative x-axis along the axis of the tube, and choose this constant so that at

$$\phi^*(\boldsymbol{x}) \sim O\left(\frac{1}{|\boldsymbol{x}|}\right) \to 0 \quad \text{as} \quad |\boldsymbol{x}| \to \infty \quad \text{outside the tube.} \tag{1.3}$$

Then $\phi^*\nabla\phi^* \sim 1/|\boldsymbol{x}|^3$ as $|\boldsymbol{x}| \to \infty$ outside the tube, and (1.1) and the divergence theorem imply that

$$\int_V (\nabla\phi^*)^2 \, \mathrm{d}^3\boldsymbol{x} = -\int_{S_p} \phi^* \frac{\partial\phi^*}{\partial x} \, \mathrm{d}y \, \mathrm{d}z \equiv \mathscr{A}(\ell + \ell'), \tag{1.4}$$

where the second integration is over the face S_p of the piston at $x = -\ell$. When $-x$ greatly exceeds $\mathscr{A}^{1/2}$ within the tube, the fluid motion is sensibly uniform at unit velocity parallel to the tube, and (1.4) yields

$$\phi^*(\boldsymbol{x}) \sim x - \ell' \quad \text{as} \quad x \to -\infty \ \text{ in the tube.} \tag{1.5}$$

The function ϕ^* plays an important role in the calculation of sound generated by sources in the neighbourhood of the open end of the tube, provided the frequency is sufficiently small that the characteristic acoustic wavelength is much larger than the tube diameter. The velocity potential $\varphi(\boldsymbol{x}, t)$ of the sound generated by a distribution of volume sources $q(\boldsymbol{x}, t)$ is governed by the inhomogeneous wave equation

$$\left(\frac{1}{c_o^2}\frac{\partial^2}{\partial t^2} - \nabla^2\right)\varphi = -q(\boldsymbol{x}, t), \tag{1.6}$$

where c_o is the speed of sound. The solution with outgoing wave behaviour can be expressed in the form

$$\varphi(\boldsymbol{x}, t) = -\iint G(\boldsymbol{x}, \boldsymbol{x}'; t - \tau)\, q(\boldsymbol{x}', \tau) \, \mathrm{d}^3\boldsymbol{x}' \, \mathrm{d}\tau, \tag{1.7}$$

where Green's function $G(\boldsymbol{x}, \boldsymbol{x}'; t-\tau)$ is the solution of (1.6) when the right-hand side is replaced by $\delta(\boldsymbol{x}-\boldsymbol{x}')\delta(t-\tau)$. The integrations in (1.7) are over the whole of the fluid and all times τ, and the normal derivatives of G satisfy $\partial G/\partial x_n = 0$ and $\partial G/\partial x'_n = 0$ respectively when the field points $\boldsymbol{x}$, $\boldsymbol{x}'$ lie on the rigid interior or exterior surfaces of the tube.

When the tube is semi-infinite (extending to $x = -\infty$), the sound radiated into the

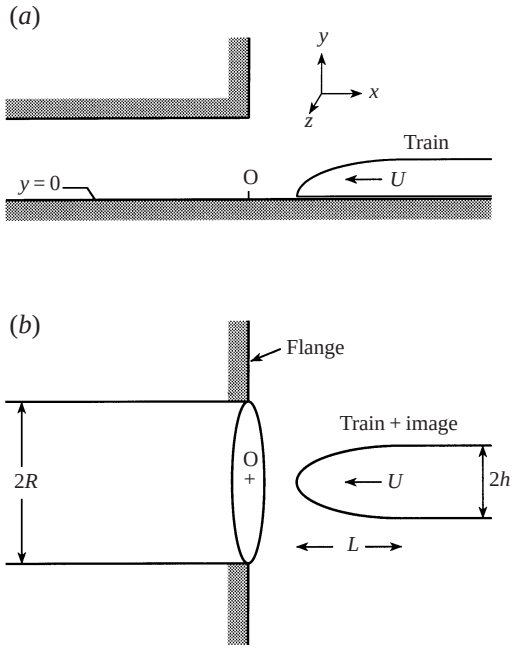

FIGURE 1. (*a*) Train entering tunnel. (*b*) Dynamically equivalent configuration consisting of the train and its image in the ground plane entering a flanged tube formed by the reflection of the tunnel walls in the ground plane. The dimensions L and h are discussed in § 4.2.

tube, produced by the interaction of low-frequency sources q with the open end is determined by the following compact approximation to G (Howe 1998*a*):

$$G(\boldsymbol{x},\boldsymbol{x}';t-\tau)\approx\frac{c_o}{2\mathscr{A}}\big\{\mathrm{H}(t-\tau-|\phi^*(\boldsymbol{x})-\phi^*(\boldsymbol{x}')|/c_o)\\ -\mathrm{H}(t-\tau+(\phi^*(\boldsymbol{x})+\phi^*(\boldsymbol{x}'))/c_o)\big\},\tag{1.8}$$

where $\mathrm{H}(x)=0,\ 1$ according as $x\lessgtr 0$ is the Heaviside step function. This formula is applicable provided that the acoustic wavelength greatly exceeds the tube diameter. It is uniformly valid when regarded as a function of either $\boldsymbol{x}$ or $\boldsymbol{x}'$ provided at least one of these points lies within the tube at a distance from the opening large compared to the diameter.

The approximation (1.8) has been applied to determine the compression wave generated when a high-speed train, depicted schematically in figure 1(*a*), enters a long tunnel (Howe 1998*a*, *b*). The train is modelled by a distribution of volume sources of constant strength convecting in the negative x-direction at the speed U of the train, i.e.

$$q(\boldsymbol{x},t)\equiv q(x+Ut,y,z).\tag{1.9}$$

The problem is dynamically equivalent to calculating the interaction of these sources plus their images in the rigid ground plane ($y=0$ in the figure) with the open-ended duct formed by the tunnel and its image in the ground (figure 1*b*). The compression wave propagates into the tunnel, ahead of the train and emerges at the distant tunnel exit as a pressure pulse, sometimes called the *micro-pressure wave*, whose amplitude and duration are determined by the train speed on entry, its cross-sectional area relative to the tunnel, and the tunnel length (Iida *et al.* 1996; Maeda *et al.* 1993; Ozawa *et al.* 1991; Swarden & Wilson 1970; Ogawa & Fujii 1994, 1996, 1997;

Mestreau, Lohner & Aita 1993). The amplitude of the compression wave is typically of order 0.01 atmospheres for a train whose travel Mach number $M = U/c_o$ exceeds about 0.2 ($\sim$ 250 k.p.h), and the pressure rise occurs over a distance (the wavefront 'thickness') of order $D/M \sim 5D$, where D is the tunnel diameter. The strength of the micro-pressure wave is proportional to the steepness of the compression wavefront at the tunnel exit. For tunnels longer than about 3 km with modern concrete slab tracks (offering little dissipation to the propagating wave), nonlinear wave steepening can produce peak micro-pressure wave amplitudes of about 50 Pa near the exit, which is comparable to the sonic boom from a supersonic aircraft.

The principal difficulty in applying the compact approximation (1.8) to the tunnel entrance problem arises in the determination of $\phi^*(\boldsymbol{x})$. This function is known analytically for an ideal tunnel consisting of an unflanged, semi-infinite circular cylinder (Howe 1998*a*); the exact Green's function (without the assumption of compactness) is also known in this case (Levine & Schwinger 1948; Noble 1958; Howe 1998*b*), and yields predictions that are in excellent accord with model-scale tests. $\phi^*(\boldsymbol{x})$ can be determined by numerical integration of Laplace's equation for more general tunnel geometries; for example, knowledge of ϕ^* for a flanged duct would be of particular value, since this corresponds more closely with the geometry of a real tunnel portal. However, there are obvious advantages to be gained from having a representation of ϕ^* in analytic form, and in this paper we show how Rayleigh's method for estimating ℓ' supplies an approximate representation of $\phi^*(\boldsymbol{x})$ for flanged ducts of circular or rectangular cross-section. The accuracy of this procedure can be estimated by comparison with the known analytical solution for a two-dimensional duct (i.e. a duct with rectangular cross-section and infinite aspect ratio), which can be solved by the method of conformal transformation.

Rayleigh's (1926) calculation of ϕ^* for a flanged, circular cylindrical duct is summarized in § 2. The corresponding approximation for a two-dimensional duct is compared with the exact solution in § 3. The case of a flanged duct of rectangular cross-section is discussed (§ 4), and applied to determine the influence of the entrance flange and duct cross-sectional shape on the compression wave generated by a train entering a tunnel.

2. The flanged, circular cylinder

2.1. *Rayleigh's approximation for* $\phi^*(\boldsymbol{x})$

Rayleigh (1926, Appendix A) determined the approximate functional form of the solution ϕ^* of Laplace's equation, subject to the conditions (1.3), (1.5) for a flanged, semi-infinite circular cylindrical duct of radius R (figure 1*b*) by posing the following representation for the normal component of velocity in the entrance plane:

$$\frac{\partial \phi^*}{\partial x} = \alpha\left(1 + \frac{\mu r^2}{R^2} + \frac{\mu' r^4}{R^4}\right), \quad x = 0, \quad r = (y^2 + z^2)^{1/2} < R, \tag{2.1}$$

where μ, μ' are constants, and continuity requires that

$$\alpha = \frac{1}{1 + \mu/2 + \mu'/3}. \tag{2.2}$$

It was argued that, although (2.1) does not become infinite at the sharp edge ($r \to R$) of the opening (where potential theory predicts that $\partial\phi^*/\partial x \sim 1/(1 - r/R)^{1/3}$), the approximation should still supply a 'very good result' for the end correction provided

the coefficients μ and μ' are chosen to make the kinetic energy T' of (1.2) a minimum. The much simpler 'piston' approximation, obtained by setting $\alpha = 1$ and $\mu = \mu' = 0$, yields the estimate $\ell' \approx 0.85R$ (Rayleigh 1926, § 307), which is only about 4% in excess of the true value.

Within the tube

$$\phi^*(\boldsymbol{x}) = x - \ell' + \sum_{n=1}^{\infty} A_n J_0\left(\lambda_n \frac{r}{R}\right) \mathrm{e}^{\lambda_n x/R}, \quad x < 0, \quad r < R, \tag{2.3}$$

where J_ν denotes the Bessel function of order ν. This expansion satisfies the axisymmetric form of Laplace's equation, and has vanishing normal derivative on the wall $r = R$ provided λ_n is the nth positive root of $\mathrm{d}J_0(\lambda)/\mathrm{d}\lambda \equiv -J_1(\lambda) = 0$ (Abramowitz & Stegun 1970). The coefficients A_n are chosen to satisfy condition (2.1), which yields

$$A_n = \frac{4\alpha R}{\lambda_n^3 J_0(\lambda_n)} \left\{ \mu + 2\mu' \left(1 - \frac{8}{\lambda_n^2}\right) \right\}. \tag{2.4}$$

The kinetic energy T_I of the motion within the section V_I, say, of the duct contained in the interval $-\ell < x < 0$ (where $\ell \gg R$) is given by

$$\begin{aligned} \frac{2T_I}{\rho_o} &= \int_{V_I} (\nabla\phi^*)^2 \,\mathrm{d}^3\boldsymbol{x} \equiv 2\pi \int_0^R \left[\left(\phi^* \frac{\partial \phi^*}{\partial x} \right)_{x=0} - \left(\phi^* \frac{\partial \phi^*}{\partial x} \right)_{x=-\ell} \right] r \,\mathrm{d}r \\ &= \pi R^2 \left(\ell + 16\alpha^2 R \sum_{n=1}^{\infty} \frac{\left[\mu + 2\mu' \left(1 - 8/\lambda_n^2\right)\right]^2}{\lambda_n^5} \right). \end{aligned} \tag{2.5}$$

In the region $x > 0$ the flow spreads hemispherically, and

$$\phi^*(\boldsymbol{x}) = \frac{-1}{2\pi} \int_{S_o} \frac{u(y', z')\,\mathrm{d}y'\,\mathrm{d}z'}{(x^2 + (y - y')^2 + (z - z')^2)^{1/2}}, \quad x > 0, \tag{2.6}$$

where the integration is over the open end S_o of the tube, and $u = \partial\phi^*/\partial x$ is the normal velocity (2.1). The kinetic energy T_E of the exterior motion can now be calculated from the formula

$$\frac{2T_E}{\rho_o} = -\int_{S_o} \phi^* \frac{\partial \phi^*}{\partial x} \mathrm{d}y\,\mathrm{d}z. \tag{2.7}$$

(for details see Rayleigh 1926), whereupon the relation (1.2) satisfied by $T' = T_I + T_E$ becomes

$$\begin{aligned} \ell + \ell' \leqslant \frac{2}{\rho_o \mathscr{A}}(T_I + T_E) = \ell + 16\alpha^2 R \sum_{n=1}^{\infty} \frac{\left[\mu + 2\mu' \left(1 - 8/\lambda_n^2\right)\right]^2}{\lambda_n^5} \\ + \frac{8\alpha^2 R}{3\pi} \left(1 + \frac{14\mu}{15} + \frac{314\mu'}{525} + \frac{5\mu^2}{21} + \frac{214\mu\mu'}{675} + \frac{89\mu'^2}{825} \right). \end{aligned} \tag{2.8}$$

The values of μ, μ' that minimize the right-hand side are given in the first row of table 1. The corresponding estimate $\ell' = 0.8242R$ for the end correction (obtained by replacing '$\leqslant$' by '$=$' in (2.8)) is given in column three of the table, and agrees exactly with the value found by Rayleigh.

The broken line curve in figure 2 indicates that, because μ and μ' have different signs, the normal exit velocity $(\partial\phi^*/\partial x)_{x=0}$ has a maximum ~ 0.87 on the axis $r = 0$ and a minimum (~ 0.76) near $r/R = 0.5$. This behaviour is not characteristic of a potential outflow, where the velocity is expected to increase monotonically with

μ	μ'	ℓ'/R
−1.0120	1.9515	0.8242
0.0	1.1030	0.8254
1.1520	0.0	0.8281

TABLE 1. Minimizing parameter values for the flanged, circular cylinder.

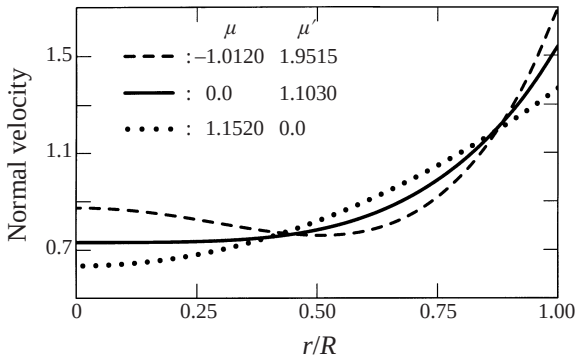

FIGURE 2. Radial distributions of the exit plane normal velocity $\partial\phi^*/\partial x$ modelled by equation (2.1).

distance from the axis. In § 3 it will be argued that this flow involves a relatively substantial distribution of vorticity in the exit plane of the duct. A more realistic exit flow is obtained by setting $\mu = 0$ and minimizing the kinetic energy (2.8) with respect to variations in μ' alone. The minimum occurs at $\mu' = 1.103$, and supplies a marginally larger estimate of the end correction (see table 1) that also agree with Rayleigh's prediction for this case. The exit velocity (solid curve in figure 2) now varies in much the expected manner, rising to a maximum at $r = R$ that is about twice that on the axis. The energy can also be minimized after setting $\mu' = 0$ (table 1, row 3; Rayleigh 1870), leading to $\ell' = 0.8281R$, but the corresponding parabolic profile of the exit velocity (dotted in figure 2) is not sufficiently flat over the axial region of the opening to be an acceptable representation of the actual motion.

2.2. *Application to compression wave generation by a high-speed train*

These results will now be applied to the problem of figure 1(*b*), to determine the compression wave generated by a train entering a tunnel with a flanged portal. The linear theory solution (1.7) determines the initial compression wave profile, prior to the onset of nonlinear steepening. It is valid several tunnel diameters ahead of the train, just after tunnel entry, where the disturbed motion is small enough that the perturbation pressure is given by the linearized relation $p = -\rho_o \partial\varphi/\partial t$. Thus, using (1.8), for $M^2 \ll 1$,

$$p(\boldsymbol{x}, t) \approx \frac{\rho_o c_o}{2\mathscr{A}} \int \{q(x' + U[t] - M\phi^*(\boldsymbol{x}'), y', z') - q(x' + U[t] + M\phi^*(\boldsymbol{x}'), y', z')\}\, \mathrm{d}^3\boldsymbol{x}', \quad (2.9)$$

where the retarded time $[t] = t + (x - \ell')/c_o$ when $|x| \gg R$.

The equivalent source distribution q vanishes except near the front and rear ends of the train, where its cross-section changes significantly. The compression wave is formed during the passage of the nose of the train into the tunnel, and this interaction may be isolated by formal consideration of a very long train, whose rear is ignored.

During the interaction the source terms q in (2.9) can be expanded in powers of the Mach number, to obtain, by integration by parts,

$$p \approx p(x,t) = \frac{-\rho_o U}{\mathscr{A}} \int \phi^*(\boldsymbol{x}') \frac{\partial q}{\partial x'}(x'+U[t], y', z')\, \mathrm{d}^3\boldsymbol{x}'$$
$$= \frac{\rho_o U}{\mathscr{A}} \int q(x'+U[t], y', z') \frac{\partial \phi^*}{\partial x'}(\boldsymbol{x}')\, \mathrm{d}^3\boldsymbol{x}', \quad |x| \gg R \quad \text{in the tunnel.} \quad (2.10)$$

Excellent agreement has been found between predictions of this formula and results of model scale tests conducted by Maeda *et al.* (1993) using a configuration similar to that shown in figure 1(*b*), but involving an unflanged circular cylinder and a 'train + image' consisting of a wire-guided, axisymmetric model projected along the axis of the cylinder (Howe 1998*a*). The profiled nose of the train was of length L, and the source distribution was approximated by the line source

$$q(\mathbf{x}) = U\mathscr{A}_o Q(x)\delta(y)\delta(z-z_\mathrm{T}), \quad Q = \frac{1}{\mathscr{A}_o}\frac{\partial \mathscr{A}_\mathrm{T}}{\partial x}(x), \quad (2.11)$$

where $\mathscr{A}_\mathrm{T}(x)$ is the cross-sectional area of the train at distance x from the nose, so that $\mathscr{A}_\mathrm{T}(L) \equiv \mathscr{A}_o$, where $\mathscr{A}_o$ is the uniform train cross-section to the rear of the nose, and the ground level line $y = 0, z = z_\mathrm{T}$ lies in the vertical plane of symmetry of the train. Then (2.10) becomes

$$p(x,t) \approx \frac{\rho_o U^2 \mathscr{A}_o}{\mathscr{A}} \int Q(x'+U[t]) \frac{\partial \phi^*}{\partial x'}(x', 0, z_\mathrm{T})\, \mathrm{d}x', \quad \text{for} \quad -x \gg R, \quad M^2 \ll 1. \quad (2.12)$$

A special case that yields an overall picture of compression wave formation is that of a long, 'snub' -nosed train with a profiled nose whose length L tends to zero. Then $q(\boldsymbol{x})$ reduces to a point source, because $Q(x) \equiv (1/\mathscr{A}_o)\,\partial\mathscr{A}_\mathrm{T}/\partial x \to \delta(x)$ as $L \to 0$, and by setting $Q(x'+U[t]) = \delta(x'+U[t])$ in (2.12) we find

$$p(x,t) = \frac{\rho_o U^2 \mathscr{A}_o}{\mathscr{A}} \left(\frac{\partial \phi^*}{\partial x'}(x', 0, z_\mathrm{T}) \right)_{x'=-U[t]}, \quad \text{for} \quad -x \gg R, \quad M^2 \ll 1. \quad (2.13)$$

The approximations (2.3) and (2.6) can be used to evaluate $\partial\phi^*/\partial x'$ in this formula respectively for $x' \lesseqgtr 0$, provided the offset z_T of the path of the train is not too large, since the approximations must fail close to the edge of the flange. The flatness of the solid curve in figure 2 over the central section of the cylinder exit suggests that such edge effects do not become important until $|z_\mathrm{T}|$ exceeds about $\frac{1}{2}R$ when $\mu = 0$, $\mu' = 1.1030$. The curve labelled 'p' in figure 3(*b*) illustrates the compression wave pressure profile for a snub-nosed train calculated for this case when $z_\mathrm{T} = 0$; it is plotted as a function of the non-dimensional retarded time $U[t]/R$, which is defined such that the nose of the train (in this case, the point source) crosses the entrance plane of the cylinder at $U[t]/R = 0$.

The compression wave 'gradient' $\partial p(x,t)/\partial t$ is frequently measured in experiments, because its magnitude at the far end of a tunnel determines the amplitude of the micro-pressure wave pulse. The present calculations determine only the initial profile of the compression wave, since the nonlinear steepening that can occur in a long tunnel is ignored. Nevertheless, if the initial pressure gradient is sufficiently small (corresponding to a compression wave with a 'long' rise time) subsequent nonlinear steepening is often inhibited by dissipative mechanisms associated, for example, with frictional losses in ballast interstices.

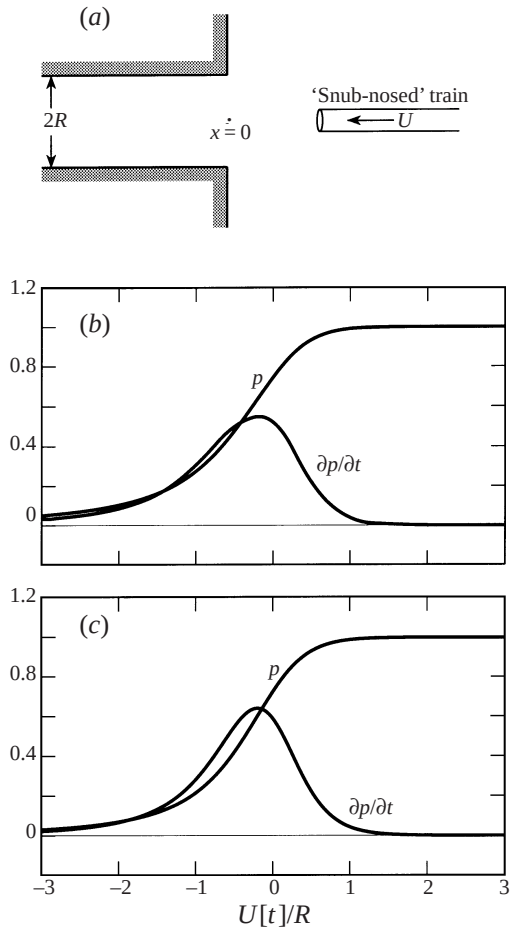

FIGURE 3. (*a*) Circular cylindrical portal with infinite flange. (*b*) Non-dimensional pressure $p/(\rho_o U^2 \mathscr{A}_o/\mathscr{A})$ and pressure 'gradient' $(\partial p/\partial t)/(\rho_o U^3 \mathscr{A}_o/\mathscr{A} R)$ for a snub-nosed train when $M^2 \ll 1$, and for $\mu = 0$, $\mu' = 1.1030$. (*c*) Corresponding pressure and pressure gradient for an unflanged cylinder.

It follows from (2.12) that the initial pressure gradient can be written

$$\frac{\partial p}{\partial t}(x,t) \approx \frac{-\rho_o U^3 \mathscr{A}_o}{\mathscr{A}} \int Q(x' + U[t]) \frac{\partial^2 \phi^*}{\partial x'^2}(x', 0, z_T)\, \mathrm{d}x', \quad \text{for} \quad -x \gg R, \quad M^2 \ll 1. \tag{2.14}$$

For the snub-nosed train this simplifies to

$$\frac{\partial p}{\partial t}(x,t) \approx \frac{-\rho_o U^3 \mathscr{A}_o}{\mathscr{A}} \left(\frac{\partial^2 \phi^*}{\partial x'^2}(x', 0, z_T) \right)_{x' = -U[t]}, \quad \text{for} \quad -x \gg R, \quad M^2 \ll 1. \tag{2.15}$$

In general the second derivative $\partial^2 \phi^*/\partial x^2$ calculated by Rayleigh's method is discontinuous across the tunnel entrance plane, because the approximation implicitly includes a distribution of vorticity over $x = 0$. Therefore, in using (2.14), (2.15) to evaluate the pressure gradient in the immediate vicinity of $x = 0$, the value of $\partial^2 \phi^*/\partial x^2$ is approximated there by the mean of its values on both sides of the discontinuity. The magnitude of the discontinuity is small, and this procedure supplies a smoothly varying pressure gradient, as indicated by the $\partial p/\partial t$ curve in figure 3(*b*).

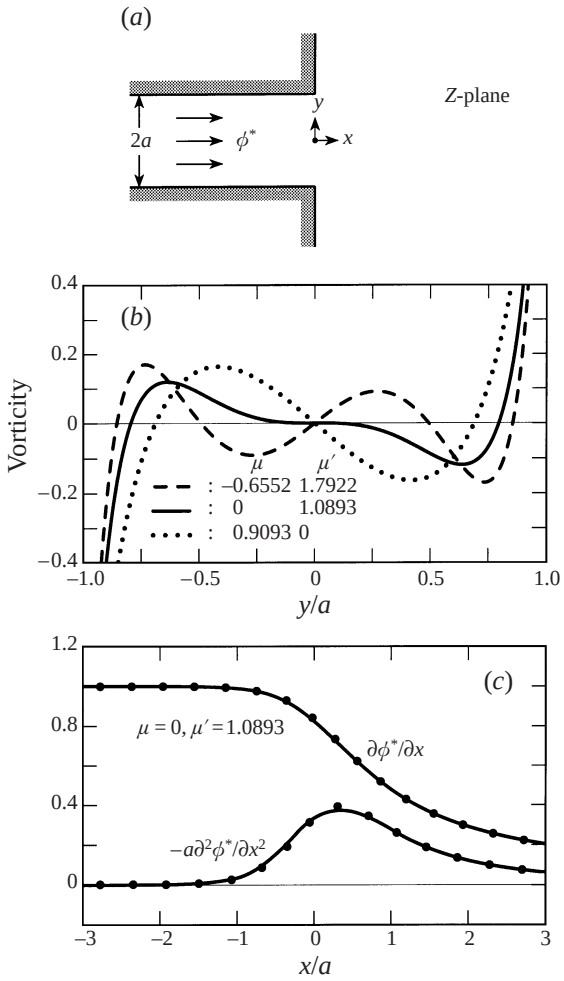

FIGURE 4. (*a*) Potential flow from a two-dimensional, flanged channel. (*b*) Exit-plane vorticity distributions when ϕ^* satisfies (3.1). (*c*) Comparison of the case (ii) approximation (——) with exact results (• • •) on the x-axis.

The influence of the tunnel entrance flange can be seen by comparison with the exact predictions for an unflanged circular cylinder (Howe 1998*a*, *b*), which are reproduced in figure 3(*c*). The flange inhibits the motion of fluid displaced by the advancing train, causing an increased rise in pressure prior to the entry of the train into the tunnel. However, because the overall pressure rises are the same in both cases, the pressure gradient is smaller for the flanged entrance, the maximum being about 85% of that for the unflanged entrance.

3. The potential ϕ^* in two dimensions

A measure of the accuracy of Rayleigh's approximation furnished by the two-parameter representation (2.1) of $\partial\phi^*/\partial x$ in the exit plane can be obtained by considering the two-dimensional problem (figure 4*a*) of flow from a uniform flanged

duct of width $2a$. However, at large distances from the opening in $x > 0$

$$\phi^* \sim \frac{2a}{\pi} \ln r, \quad r = (x^2 + y^2)^{1/2},$$

and the usual end correction does not exist, because the kinetic energy of the exterior motion is now infinite. But, the formal procedure of § 2 is still applicable, with

$$\frac{\partial \phi^*}{\partial x} = \alpha \left(1 + \frac{\mu y^2}{a^2} + \frac{\mu' y^4}{a^4}\right), \quad x = 0, \quad -a < y < a, \quad \text{where} \quad \alpha = \frac{1}{1 + \mu/3 + \mu'/5}. \tag{3.1}$$

The kinetic energies T_I, T_E of the flow are evaluated per unit span (out of the plane of the paper in the figure) respectively in the section $-\ell < x < 0$ of the duct, and within the semi-circular domain $r < \mathscr{R}$ in $x > 0$, where ℓ and $\mathscr{R}$ are both assumed to be large compared to the duct width $2a$.

To do this we set

$$\begin{aligned} \phi^*(x, y) &= \frac{\alpha}{\pi} \int_{-a}^{a} \left(1 + \frac{\mu y'^2}{a^2} + \frac{\mu' y'^4}{a^4}\right) \ln (x^2 + (y - y')^2)^{1/2} \, \mathrm{d}y', \quad x > 0, \\ &= x - \ell' + \sum_{n=1}^{\infty} A_n \cos\left(\frac{n\pi y}{a}\right) \mathrm{e}^{n\pi x/a}, \quad x < 0, \end{aligned} \tag{3.2}$$

where ℓ' may now be regarded as an arbitrary constant, and the condition (3.1) gives

$$A_n = \frac{4\alpha a(-1)^n}{n^3\pi^3} \left\{\mu + 2\mu' \left(1 - \frac{6}{n^2\pi^2}\right)\right\}. \tag{3.3}$$

Using these formulae (as in § 2) it is readily deduced that

$$\left.\begin{aligned} \frac{T_I}{\rho_o a} &= \ell + 8a\alpha^2 \sum_{n=1}^{\infty} \frac{\left[\mu + 2\mu' \left(1 - 6/n^2\pi^2\right)\right]^2}{n^5\pi^5}, \\ \frac{T_E}{\rho_o a} &= \frac{2a}{\pi} \ln\left(\frac{\mathscr{R}}{a}\right) + \frac{\alpha^2 a}{2\pi} \left(\mathscr{I}_{0,0} + 2\mu\mathscr{I}_{2,0} + 2\mu'\mathscr{I}_{4,0} + \mu^2\mathscr{I}_{2,2} + 2\mu\mu'\mathscr{I}_{4,2} + \mu'^2\mathscr{I}_{4,4}\right), \end{aligned}\right\} \tag{3.4}$$

where

$$\mathscr{I}_{i,j} = \mathscr{I}_{j,i} = -\iint_{-1}^{1} \lambda^i \xi^j \ln|\xi - \lambda| \mathrm{d}\lambda \, \mathrm{d}\xi > 0. \tag{3.5}$$

Table 2 lists the values of μ, μ' that minimize

$$\Delta = \frac{T_I + T_E}{\rho_o a^2} - \left[\frac{\ell}{a} + \frac{2}{\pi} \ln\left(\frac{\mathscr{R}}{a}\right)\right] \tag{3.6}$$

for the three different cases where (i) μ and μ' vary independently, (ii) $\mu = 0$, (iii) $\mu' = 0$.

Although the smallest value of Δ is obtained for case (i), we shall still reject this in approximating ϕ^*, because it yields a normal velocity $\partial\phi^*/\partial x$ in the exit plane of the channel that varies in the manner indicated previously by the broken-line curve in figure 2 for the corresponding approximation for the flanged, circular tube. As in § 2, we shall regard case (ii) as providing the best overall approximation to the irrotational exit flow. This choice may be justified by consideration of the discontinuity

$$\frac{\partial \phi^*}{\partial y}(+0, y) - \frac{\partial \phi^*}{\partial y}(-0, y)$$

μ	μ'	Δ
−0.6552	1.7922	0.4851
0.0	1.0893	0.4858
0.9093	0.0	0.4890

TABLE 2. Energy minimizing values for two-dimensional flow.

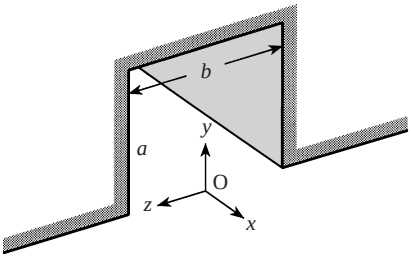

FIGURE 5. Rectangular tunnel portal.

in the transverse component of velocity. This is just the strength of the vortex sheet that must span the channel exit when $\partial\phi^*/\partial x$ is approximated by (3.1), and would vanish if (3.1) were exact. It is plotted for all three cases in figure 4(*b*). The vorticity is logarithmically large at the edges, but there are also significant distributions of vorticity near the axis of the channel in cases (i) and (iii), whereas for case (ii) the vorticity is confined to the outer regions. In particular, this implies for case (ii) that, in the neighbourhood of $y = 0$, the magnitude of the discontinuity in $\partial^2\phi^*/\partial x^2$ at $x = 0$ will tend to be small.

The solid curves in figure 4(*c*) indicate the variations of $\partial\phi^*/\partial x$ and $\partial^2\phi^*/\partial x^2$ along the duct axis calculated from the approximation (3.2) in case (ii). The value of $\partial^2\phi^*/\partial x^2$ at $x = 0$ is obtained by averaging values on either side of the discontinuity, as described in § 2. But, these quantities can also be calculated exactly, and are plotted as dotted curves in figure 4(*c*), from the relations

$$\phi^*(x, y) = \mathrm{Re}\ (w), \quad w = \frac{2a}{\pi} \ln \zeta(Z), \tag{3.7}$$

where $Z = x + \mathrm{i}y$. The two-dimensional fluid region bounded by the flanged channel is mapped onto the upper half of the ζ-plane by

$$Z = \frac{2a}{\pi} \left\{ \ln\left[1 + \mathrm{i}(\zeta^2 - 1)^{1/2}\right] - \ln \zeta - \mathrm{i}(\zeta^2 - 1)^{1/2} \right\} - \mathrm{i}a, \tag{3.8}$$

where the outflow is equivalent to that from a source of strength $2a$ at $\zeta = 0$.

This comparison shows that case (ii) of Rayleigh's method yields excellent approximations for both $\partial\phi^*/\partial x$ and $\partial^2\phi^*/\partial x^2$, even close to the exit plane $x = 0$.

4. Tunnel with rectangular portal

4.1. *Calculation of* ϕ^*

Rayleigh's method is next applied to a tunnel of rectangular cross-section, with a flanged portal of height a and width b, as illustrated schematically in figure 5. ϕ^* describes potential flow from a rectangular duct of cross-section $2a \times b$ obtained by

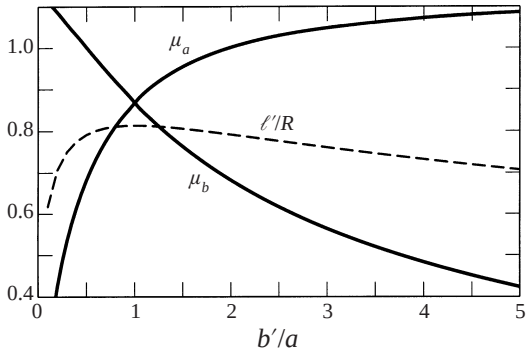

FIGURE 6. Dependence on b'/a of μ_a, μ_b and the end correction ℓ' normalized by the radius R of the circular cylinder whose cross-sectional area equals that of the rectangular duct ($\pi R^2 = 2ab$, $b = 2b'$).

removing the ground plane and introducing the image of the tunnel in $y = 0$. The results of §§ 2, 3 strongly imply that an efficient approximation is obtained by setting

$$\frac{\partial \phi^*}{\partial x} = \alpha\left(1 + \frac{\mu_a y^4}{a^4} + \frac{\mu_b z^4}{b'^4}\right), \quad \text{for} \quad x = 0,$$

where

$$\alpha = \frac{1}{1 + (\mu_a + \mu_b)/5} \quad \text{and} \quad b' = \frac{b}{2}. \tag{4.1}$$

Then $\phi^*(\boldsymbol{x})$ is given by an integral of the form (2.6) in the region $x > 0$ outside the tunnel, where $u(y, z)$ is the exit-plane velocity defined by (4.1). Within the tunnel (in $x < 0$) the appropriate solution of Laplace's equation is

$$\phi^*(\boldsymbol{x}) = x - \ell' + \sum_{n=1}^{\infty} \frac{8\alpha(-1)^n}{n^3\pi^3}\left(1 - \frac{6}{n^2\pi^2}\right) \times \left\{a\mu_a \cos\left(\frac{n\pi y}{a}\right) e^{n\pi x/a} + b'\mu_b \cos\left(\frac{n\pi z}{b'}\right) e^{n\pi x/b'}\right\}, \tag{4.2}$$

where ℓ' is the end correction.

The analogue of the energy relation (2.8) is

$$\ell' \leqslant 32\alpha^2(a\mu_a^2 + b'\mu_b^2)\sum_{n=1}^{\infty} \frac{1}{n^5\pi^5}\left(1 - \frac{6}{n^2\pi^2}\right)^2 + \frac{\alpha^2 a^2}{8\pi b'} \times (\hat{\mathscr{I}}_{0,0,0,0} + 2\mu_a \hat{\mathscr{I}}_{4,0,0,0} + 2\mu_b \hat{\mathscr{I}}_{0,0,4,0} + 2\mu_a\mu_b \hat{\mathscr{I}}_{4,0,4,0} + \mu_a^2 \hat{\mathscr{I}}_{4,4,0,0} + \mu_b^2 \hat{\mathscr{I}}_{0,0,4,4}), \tag{4.3}$$

where

$$\hat{\mathscr{I}}_{i,j,k,l} = \left(\frac{a}{b'}\right)^{k+l} \int\!\!\int_{-1}^{1} d\xi\, d\eta \int\!\!\int_{-b'/a}^{b'/a} \frac{\xi^i \eta^j \lambda^k \chi^l\, d\lambda\, d\chi}{((\xi - \eta)^2 + (\lambda - \chi)^2)^{1/2}}. \tag{4.4}$$

The two terms on the right of (4.3) correspond respectively to the contributions to the kinetic energy of the exit flow (i.e. the end correction) from the interior ($x < 0$) and exterior ($x > 0$) regions. The values of μ_a and μ_b that minimize the right-hand side of (4.3) are plotted in figure 6 against b'/a, and listed in table 3. Note that

b'/a	μ_a	μ_b	ℓ'/R	b'/a	μ_a	μ_b	ℓ'/R
1.00	0.868	0.868	0.813	3.25	1.056	0.541	0.753
1.25	0.919	0.812	0.811	3.50	1.062	0.520	0.746
1.50	0.955	0.763	0.806	3.75	1.068	0.501	0.739
1.75	0.981	0.720	0.799	4.00	1.073	0.483	0.732
2.00	1.001	0.682	0.792	4.25	1.077	0.467	0.725
2.25	1.017	0.648	0.784	4.50	1.081	0.451	0.719
2.50	1.030	0.617	0.776	4.75	1.084	0.437	0.713
2.75	1.040	0.589	0.768	5.00	1.086	0.424	0.707
3.00	1.049	0.564	0.761				

TABLE 3. Energy minimizing values for a rectangular portal ($b' = \frac{1}{2}b$).

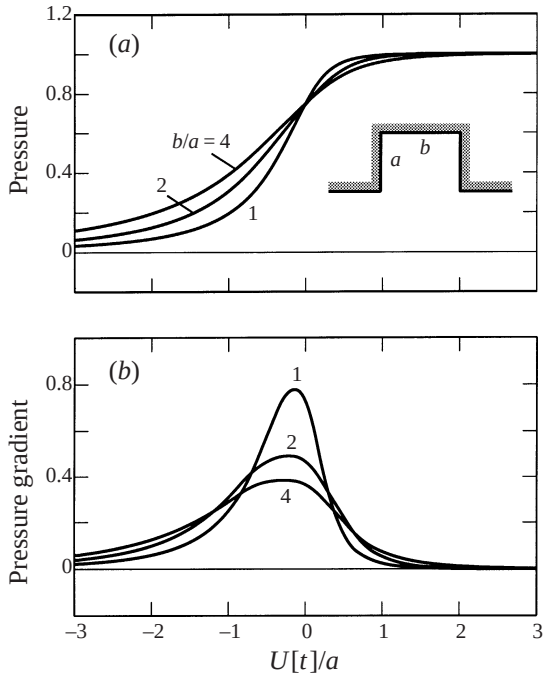

FIGURE 7. (*a*) Non-dimensional pressure $p/(\rho_o U^2 \mathscr{A}_o/\mathscr{A})$ and (*b*) pressure 'gradient' $(\partial p/\partial t)/(\rho_o U^3 \mathscr{A}_o/\mathscr{A}a)$ for a snub-nosed train entering a flanged, rectangular cylindrical tunnel when $M^2 \ll 1$ and aspect ratios $b/a = 1, 2, 4$.

$\mu_{a,b}(b'/a) = \mu_{b,a}(a/b')$. The broken line curve in the figure is the ratio ℓ'/R of the end correction to the radius $R = (2ab/\pi)^{1/2}$ of the circular cylindrical duct of the same cross-sectional area. The end correction for a flanged circular cylinder $\approx 0.82R$, and the figure and table 3 show that the end correction of the rectangular duct is within 15% of that for a circular duct of the same cross-section for b'/a as large as 5.

4.2. *The compression wave*

The dependences on the tunnel aspect ratio b/a of the compression wave pressure profile $p(x,t)$ and pressure 'gradient' $\partial p(x,t)/\partial t$ are illustrated in figure 7 for a snub-

nosed train modelled by a point source entering the tunnel along the x-axis, where they are plotted against the non-dimensional retarded time $U[t]/a$. These results demonstrate how the initial waveform progressively steepens as the width b of the tunnel decreases. They are calculated from equations (2.13) and (2.15) for $M^2 \ll 1$ and $z_T = 0$, when $\phi^*(\boldsymbol{x})$ is defined by (4.2) within the tunnel and by (2.6) outside. The values of μ_a, μ_b for the square portal, for which $b/a = 1$, are obtained by interchanging the values given in table 3 for $b'/a = 2$.

Model-scale measurements have been made of the pressure and pressure gradient of the compression wave generated when an axisymmetric, wire-guided model 'train' is projected along the axis of a 7 m long, unflanged circular cylinder of radius $R = 0.0735$ m (Maeda *et al.* 1993). This corresponds to the situation illustrated in figure 1(*b*), but in the absence of the flange, where the axisymmetric projectile represents the train and its image in the ground plane. The train nose profiles (of length L) included the cone, and the paraboloid and ellipsoid of revolution with respective cross-sectional areas

$$\frac{\mathscr{A}_T(x)}{\mathscr{A}_o} = \begin{cases} x^2/L^2, & x/L, \quad x/L\left(2 - x/L\right), & 0 < x < L, \\ 1, & & x \geqslant L, \end{cases} \tag{4.5}$$

where x is measured from the tip of the nose, and $\mathscr{A}_o = \pi h^2$, where h is the radius of the uniform section of the axisymmetric model train to the rear of the profiled nose. The corresponding source densities Q, defined as in (2.11), are given by

$$Q(x) = \begin{cases} 2x/L^2, & 1/L, \quad 2/L\left(1 - x/L\right), & 0 < x < L, \\ 0, & & \text{elsewhere.} \end{cases} \tag{4.6}$$

The values of the 'pressure gradient $\partial p/\partial t$ measured at 1 m from the tunnel entrance plane were found to be about 8% larger than the small Mach number approximation (2.14) (see Howe 1998*a*, who used the known, analytic form of the potential ϕ^* for an unflanged circular cylinder) for the following parameter values:

$$\frac{h}{L} = 0.2, \quad \frac{\mathscr{A}_o}{\mathscr{A}} = 0.116, \quad M = 0.19.$$

In figure 8(*a–c*) we compare the pressure gradient profiles for these same parameter values for three different tunnels: (*a*) the square portal, corresponding to $b/a = 1$ in figure 7; (*b*) the flanged, circular cylindrical tunnel of radius R of § 2; (*c*) the unflanged circular cylindrical tunnel of Howe (1998*a*). The tunnels have equal cross-sectional areas (i.e. $\pi R^2 = 2a^2$ or $a = R(\pi/2)^{1/2}$) and retarded times are all taken in the non-dimensional form $U[t]/R$, and the pressure gradients are normalized as

$$\left(\frac{R\mathscr{A}}{\rho_o U^3 \mathscr{A}_o}\right)\frac{\partial p}{\partial t}.$$

In all cases the profiles are determined by equation (2.15) with $z_T = 0$. The pressure gradient profiles are qualitatively the same for all three tunnels, and exhibit a remarkably weak dependence on portal geometry. The largest peak values occur for the unflanged circular cylinder (*c*), which are between 6 and 10% larger than the corresponding peaks for the flanged circular cylinder, and about 3% larger than those for the square portal. The differences in predictions for the different nose shapes for the same tunnel are discussed by Howe (1998*a*).

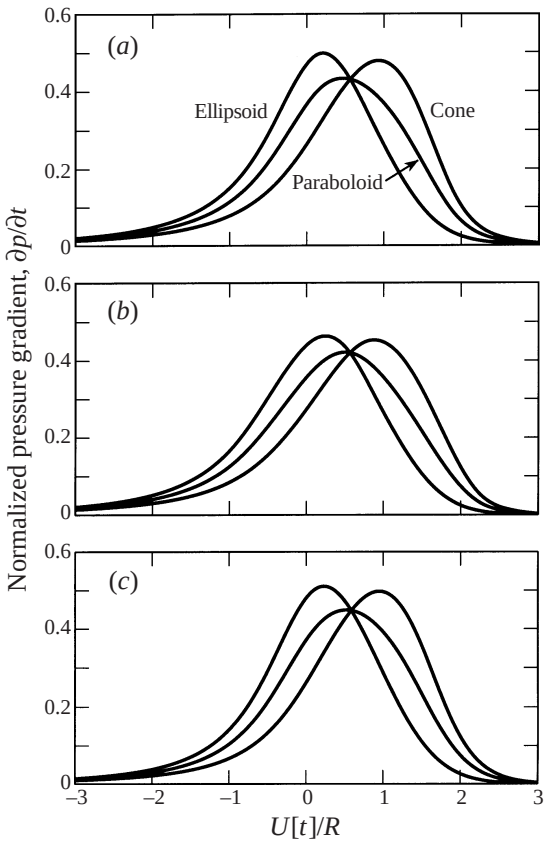

FIGURE 8. Non-dimensional pressure 'gradient' $(\partial p/\partial t)/(\rho_o U^3 \mathscr{A}_o/\mathscr{A}R)$ for axisymmetric model trains with conical, paraboloidal and ellipsoidal nose profiles, for $M^2 \ll 1$, $h/L = 0.2$ and $\mathscr{A}_o/\mathscr{A} = 0.116$: (*a*) square portal; (*b*) flanged, circular cylinder; (*c*) unflanged circular cylinder. The tunnels have equal cross-sectional areas and all lengths are non-dimensionalized by the radius R of the circular cylinder (so that $a = R(\pi/2)^{1/2}$).

5. Conclusion

Rayleigh derived an accurate value for the end correction for a flanged circular cylinder by application of Kelvin's minimum energy principle to estimate an approximate analytic form for the potential of irrotational flow from the cylinder. The particular potential ϕ^* that represents flow at unit speed deep inside the cylinder also occurs in the Green's function that governs the generation of pressure waves within the cylinder by sources near the cylinder entrance. Such waves are produced when a high-speed train enters a tunnel. Uniformly translating monopole sources of constant strength can be used to model the displacement of air by the train, and Rayleigh's method can be used to obtain an analytic representation of the compression wave. The procedure has been demonstrated for flanged, cylindrical tunnels of semi-circular and rectangular cross-section, for which exact analytic representations of ϕ^* are not available. It has been justified by comparison of Rayleigh's approximation for ϕ^* for a two-dimensional flanged duct with the exact solution obtained by the method of conformal transformation.

The specific results and illustrations given in this paper are strictly valid for train Mach numbers satisfying $M^2 \ll 1$. However, it has been shown by Howe (1998*c*) that

predictions derived for low Mach numbers can be extrapolated to values of M as large as 0.4 by the following modified form of (2.14):

$$p(x,t) \approx \frac{\rho_o U^2 \mathscr{A}_o}{(1-M^2)\mathscr{A}} \int Q(x' + U[t]) \frac{\partial \phi^*}{\partial x'}(x', 0, z_T)\, \mathrm{d}x', \tag{5.1}$$

where $\phi^*(\boldsymbol{x})$ may be approximated by Rayleigh's method.

REFERENCES

Abramowitz, M. & Stegun, I. A. 1970 (Eds.) *Handbook of Mathematical Functions* (Ninth corrected printing). National Bureau of Standards.

Howe, M. S. 1998*a* The compression wave produced by a high-speed train entering a tunnel. *Proc. R. Soc. Lond.* A **454**, 1523–1534.

Howe, M. S. 1998*b* Mach number dependence of the compression wave generated by a high-speed train entering a tunnel. *J. Sound Vib.* **212**, 23–36.

Howe, M. S. 1998*c* On the compression wave generated when a high-speed train enters a tunnel with a flared portal. *J. Fluids Structures* (in press).

Iida, M., Matsumura, T., Nakatani, K., Fukuda, T. & Maeda, T. 1996 Optimum nose shape for reducing tunnel sonic boom. *Institution of Mechanical Engineers Paper* C514/015/96.

Lamb, H. 1932 *Hydrodynamics* (6th edn.). Cambridge University Press (Reprinted 1993).

Levine, H. and Schwinger, J. 1948 On the radiation of sound from an unflanged circular pipe. *Phys. Rev.* **73**, 383–406.

Maeda, T., Matsumura, T., Iida, M., Nakatani, K. & Uchida, K. 1993 *Effect of shape of train nose on compression wave generated by train entering tunnel. Proceedings of the International Conference on Speedup Technology for Railway and Maglev Vehicles* (Yokohama, Japan 22-26 November), pp. 315–319.

Mestreau, E., Lohner, R. & Aita, S. 1993 TGV tunnel entry simulations using a finite element code with automatic remeshing. *AIAA Paper* 93–0890.

Noble, B. 1958 *Methods based on the Wiener–Hopf Technique*. Pergamon (reprinted 1988 by Chelsea Publishing Company, New York).

Ogawa, T. & Fujii, K. 1994 Numerical simulation of compressible flows induced by a train moving into a tunnel. *Comput. Fluid Dyn. J.* **3**, 63–82.

Ogawa, T. & Fujii, K. 1996 Prediction and alleviation of a booming noise created by a high-speed train moving into a tunnel. In *Proc. European Community Conf. on Computational Methods in Applied Sciences*. John Wiley and Sons.

Ogawa, T. & Fujii, K. 1997 Numerical investigation of three dimensional compressible flows induced by a train moving into a tunnel. *J. Computers Fluids* **26**, 565–585.

Ozawa, S., Maeda, T., Matsumura, T., Uchida, K., Kajiyama, H. & Tanemoto, K. 1991 Countermeasures to reduce micro-pressure waves radiating from exits of Shinkansen tunnels. In *Aerodynamics and Ventilation of Vehicle Tunnels*, pp. 253–266 Elsevier.

Rayleigh, Lord 1870 On the theory of resonance. *Phil. Trans. R. Soc. Lond.* **161**, 77–118 (also *Scientific Papers*, Vol. 1, pp. 33–75, Dover, 1964).

Rayleigh, Lord 1926 *The Theory of Sound*, Vol. 2. Macmillan.

Swarden, M. C. & Wilson, D. G. 1970 Vehicle-tunnel entry at subsonic speeds. Final Report – Part 1. *Rep.* DSR 76111-3. Engineering Projects Laboratory, Department of Mechanical Engineering, Massachusetts Institute of Technology.